

Injection-Based Online Capacitance Monitoring With Optimal Selection of Injection Frequency in Buck Converters

Xinguo Zhang, *Student Member, IEEE*, Kang Yue[✉], *Student Member, IEEE*,
Haoyu Wang[✉], *Senior Member, IEEE*, Junrui Liang[✉], *Senior Member, IEEE*,
and Yu Liu[✉], *Senior Member, IEEE*

Abstract—The aging process of aluminum electrolytic capacitors leads to a reduction in capacitance, which affects the safe operation of switching power converters. This article proposes an online capacitance monitoring method of Buck converters with high capacitance estimation accuracy. The proposed method does not ask for specific operating condition of the circuit, and does not need to model complex circuit dynamics in time domain. With the measurement errors considered, the article mathematically proves that the minimum error of capacitance estimation can be achieved with maximum sensitivity. Without interrupting the operation of the original system, a small disturbance with a certain frequency is injected to the duty cycle of the switches, to generate additional information for capacitance estimation. To achieve optimal sensitivity for capacitance estimation, the injection frequency is selected as the characteristic frequency based on the transfer function for capacitance estimation. Different candidates of transfer functions are also compared and evaluated to achieve minimum capacitance estimation error. Simulation and hardware experiments verify that optimal parameter sensitivity of capacitance can be achieved at the characteristic injection frequency, and the capacitance can be accurately estimated based on the proposed method.

Index Terms—Aluminum electrolytic capacitor, Buck converter, capacitance monitoring, characteristic injection, optimal sensitivity.

I. INTRODUCTION

SWITCH-MODE power converters are widely applied in renewable energy, transportation electrification, data communication, and industrial electrification [1]. Reliability of power converters is vital for safe operation of various systems [2], [3], [4]. Aluminum electrolytic capacitors are widely

Manuscript received 29 December 2023; revised 18 March 2024; accepted 29 April 2024. Date of publication 9 May 2024; date of current version 26 February 2025. This work was supported in part by the National Natural Science Foundation of China under Grant 52377114; and in part by the Key Laboratory of Control of Power Transmission and Conversion (SJTU), Ministry of Education under Grant 2022AB01. Recommended for publication by Associate Editor Ilhem Slama-Belkhdja. (*Corresponding author: Yu Liu.*)

Xinguo Zhang is with the School of Information Science and Technology, ShanghaiTech University, Shanghai 201210, China, also with Shanghai Advanced Research Institute, Chinese Academy of Sciences, Beijing 100045, China, and also with the University of the Chinese Academy of Sciences, Beijing 101408, China.

Kang Yue, Haoyu Wang, Junrui Liang, and Yu Liu are with the School of Information Science and Technology, ShanghaiTech University, Shanghai 201210, China (e-mail: liuyu@shanghaitech.edu.cn).

Color versions of one or more figures in this article are available at <https://doi.org/10.1109/JESTPE.2024.3399239>.

Digital Object Identifier 10.1109/JESTPE.2024.3399239

used in power electronic converter devices to obtain stable voltage due to their large capacity and low cost. However, volatilization of the electrolyte during long-term operation will decrease the capacitance value of aluminum electrolytic capacitors. According to research [5], [6], [7], the 20% capacitance attenuation marks the end of life of the capacitor. Therefore, it is of great importance to accurately estimate the capacitance of the electrolytic capacitor, to ensure reliable operation of converters.

Capacitance monitoring methods can be further classified into offline and online methods. The main disadvantage of **offline methods** is that it usually interrupts normal operation of converters. For example, [8] proposes a simple offline equivalent series resistance (ESR) and capacitance estimation method by adding sinusoidal waveforms. Therefore, to ensure continuous operation of converters, **online methods** have been proposed. The steady state ripple information at switching frequency is commonly used to estimate parameters [9], [10], [11], [12]. For Boost-PFC circuit in [9] and ac-dc-ac PWM converter in [10], the ac components can also be used to achieve ESR and capacitance estimation. However, the ripple information sometimes may not be adequate for accurate parameter estimation due to sensitivity issues. That is to say, large change of capacitance will cause only small change of measurements, or equivalently, small measurement errors could cause large capacitance estimation error. A detailed explanation can be found in Section II-A. To introduce additional information (information in addition to steady state components at switching frequency and its harmonics) to the parameter estimation problem, researchers propose two groups of methods: abrupt change-based methods and active injection-based methods. First, abrupt change-based methods use dynamics of the circuit generated by external triggering behavior, such as load change or circuit start-up. Dynamic state or parameter estimation methods are generally used to perform online estimation of parameters [13], [14], [15], [16], [17]. For example, [13] adopts state space model combined with PSO algorithm and digital twin to estimate all circuit parameters. However, the abrupt changes are typically based on a time sequence of specific operating conditions of the system. Therefore, researchers also propose methods based on active injection of signals. The pseudorandom binary sequence (PRBS) can generate a frequency-rich signal for parameter identification [18], [19], [20]. The injection-based

methods generate signals within a wide frequency range, and the dynamic time domain model is still required. However, the key frequency that enables accurate parameter estimation still requires further studies. To this end, injection-based methods with one specific frequency are also presented. Ahmad et al. [21] estimates the low-frequency impedance of the aluminum electrolytic capacitor at 120 Hz according to manufacturers. Li et al. [22] propose an online condition monitoring method for the dc-link capacitors applied in ac/dc/ac PWM converters based on the signal injection. The injection frequency is selected to minimize the total harmonic distortion (THD).

To sum up, compared to offline methods, online methods can estimate parameters without interruption of normal operation. Methods with active injection of signals are promising as they can bring additional information at the injection frequency to the parameter estimation problem. However, for the selection of injection frequency, one may rely on trial and error to find a frequency that works for their specific situation. Moreover, selection of the transfer function for parameter estimation is typically empirical as well. Theoretical guidelines on the selections of the injection frequency and the transfer function for parameter estimation still require careful investigation.

To this end, this article proposes a characteristic frequency injection-based method to estimate capacitance parameters. First, the concept of sensitivity is introduced and the parameter estimation challenges using original steady-state ripples are analyzed. Next, additional frequency information is injected by superimposing small perturbations on the duty cycle, and a method for characteristic frequency selection based on optimal sensitivity is proposed. In addition, among different candidates of transfer functions, a specific transfer function is selected based on optimal parameter sensitivity. The analytical expressions of capacitance estimation are given based on the selected transfer function. Finally, simulation and hardware experiments confirm that the optimal sensitivity can be achieved with the selected transfer function and the characteristic frequency. The value of capacitance can be more accurately estimated compared to cases with injections at other frequencies or using other transfer functions.

The contributions of this article are also summarized.

- 1) The relationship between the sensitivity and the accuracy of capacitance parameter estimation is theoretically analyzed, to show the importance to optimize parameter sensitivity.
- 2) The proposed method with injection at the characteristic frequency achieves optimal sensitivity and more accurate capacitance estimation results.
- 3) The influence of different transfer functions on capacitance parameter estimation is analyzed, and transfer function with optimal sensitivity is also provided.
- 4) The proposed method only requires small perturbation on the duty cycle; it does not require specific operating condition of the circuit, i.e., abrupt load change or start-up, and does not need to model complex circuit dynamics in time domain.

The remainder of this article is arranged as follows. Section II discusses the sensitivity problem in the Buck circuit,

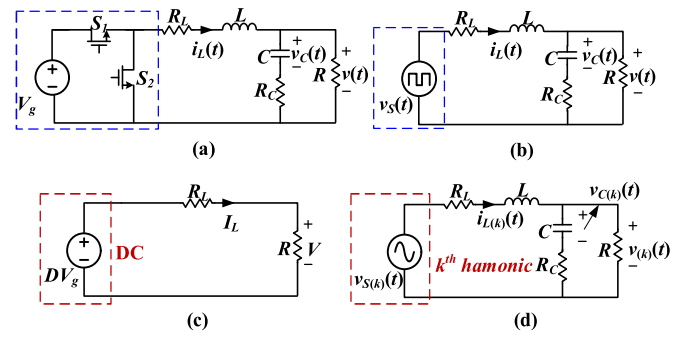


Fig. 1. Analysis of the Buck circuit. (a) Original buck circuit. (b) Buck circuit with an equivalent square wave source. (c) Buck circuit with the dc source. (d) Buck circuit with the k th harmonic source.

TABLE I
DEFINITION OF VARIABLES

Symbol	Name	Symbol	Name
$v_s(t)$	Square wave source	$v_{s(k)}(t)$	k^{th} harmonic source
$i_L(t)$	Inductor current	$v(t)$	Output voltage
I_L	DC inductor current	V	DC output voltage
$i_{L(k)}(t)$	k^{th} harmonic inductor current	$v_{(k)}(t)$	k^{th} harmonic output voltage

TABLE II
DEFINITION OF PARAMETERS

Symbol	Name	Values	Unit
R	Load resistor	7	Ω
R_L	ESR of the inductor	0.27	Ω
L	Inductor	31	μH
R_C	ESR of the capacitor	0.6	Ω
C	Capacitor	520	μF
V_g	Input voltage	5	V
D	Constant duty cycle	0.5	-
f_s	Switching frequency	200k	Hz

and the way to select optimal injection frequency and transfer function is proposed. Sections III and IV verify the proposed method by the simulation and hardware experiments. Section V draws a conclusion.

II. OPTIMAL SELECTION OF INJECTION FREQUENCY AND TRANSFER FUNCTION FOR OPTIMAL SENSITIVITY

A. Modeling and Sensitivity Analysis for Buck Converters

The circuit diagram of the Buck converter is shown in Fig. 1(a), with two switches S_1 and S_2 . The blue dotted box in Fig. 1(a) can be equivalently represented as a square wave source, as shown in Fig. 1(b). The square wave source includes dc component and k th harmonic components (where k is an integer), as shown in Fig. 1(c) and (d). The definitions of variables are provided in Table I. An example set of parameters is given in Table II, where the input voltage V_g and the duty cycle D are constants. In the Buck circuit, $v(t)$ and $i_L(t)$ are typically selected as measurements.

First, consider the circuit with the equivalent dc source as shown in Fig. 1(c). The inductor branch can be considered as a short circuit and the capacitor branch can be considered as an open circuit. The values of I_L and V can be calculated as (1). One can observe that the dc component does not contain any information about the capacitance parameters, i.e., they cannot

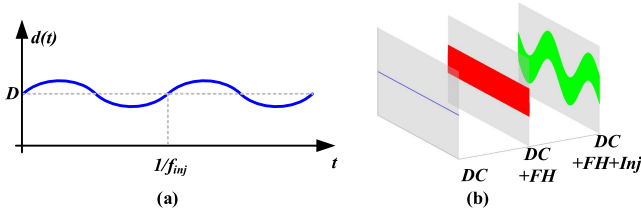


Fig. 2. Injection signal waveforms and different frequency components for Buck converters. (a) Sinusoidal perturbation on steady duty cycle. (b) Different components for Buck converter with the injection signal.

be utilized for capacitance parameter estimation

$$\begin{aligned} I_L &= DV_g / (R + R_L) \\ V &= DV_g R / (R + R_L). \end{aligned} \quad (1)$$

Next, the sensitivity issue of the capacitance estimation method using the ripple information is analyzed. Consider the circuit with the equivalent k th harmonic source as shown in Fig. 1(d). This part corresponds to the ripples (ac components) of voltages and currents within the system. $\omega_s = 2\pi f_s$ is the angular switching frequency of the system. Since the circuit operates in sinusoidal steady state, the phasor domain analysis can be adopted. Define $\tilde{Q}_{(k)}$ as the phasor representation of $q_{(k)}(t)$, where $q_{(k)}$ represents $v_{S(k)}$, $i_{L(k)}$, $v_{(k)}$ or $v_{C(k)}$. With the measurements $\tilde{V}_{(k)}$ and $\tilde{I}_{L(k)}$, the impedance value $Z_{(k)}$ can be calculated as $Z_{(k)} = \tilde{V}_{(k)} / \tilde{I}_{L(k)} = (R_C + 1/jk\omega_s C) \parallel R$, where the operator “ \parallel ” means the two elements in parallel. When $k = 1$, since the switching frequency is typically high (about tens or hundreds of kHz), the impedance of the capacitor will be small (in the order of milliohms). Intuitively, the impedance of the capacitor at the switching frequency ($k = 1$) is too small to affect the value of $Z_{(k)}$. In other words, $Z_{(k)}$ cannot accurately indicate the variation of capacitance. Similarly, when considering higher harmonics ($k > 1$), the impedance of the capacitor is even smaller, and $Z_{(k)}$ is even less sensitive to changes of capacitance parameters.

To sum up, if the system is during steady state operation at the switching frequency, it is challenging to accurately estimate capacitance using dc or harmonic (ripple, ac component) information. The essence of sensitivity issue is that, the available measurements cannot sensitively reflect the change of capacitance.

B. Injection to Duty Cycle for Additional Information

Here, a sinusoidal perturbation $d_{inj}(t) = \varepsilon_{inj} \sin(\omega_{inj}t)$ is injected to the constant duty cycle D , where $\omega_{inj} = 2\pi f_{inj}$, and ε_{inj} ($\varepsilon_{inj} \ll D$) and f_{inj} ($f_{inj} \ll f_s$) are the amplitude and frequency of the duty cycle perturbation. The duty cycle becomes $d(t) = D + d_{inj}(t)$ as depicted in Fig. 2(a). Here the magnitude of perturbation ε_{inj} is very small and does not affect normal operation of the converter.

With the duty cycle $d(t) = D + d_{inj}(t)$ and the assumptions $\varepsilon_{inj} \ll D$ and $f_{inj} \ll f_s$, the detailed expression of $v_S(t)$ can be derived as $v_S(t) = DV_g + \sum_{k=1}^{\infty} V_g / (k\pi) \cdot (1 - \cos(2\pi kD)) \sin(k\omega_s t) + v_{S,inj}(t)$, where $v_{S,inj}(t) = V_g \varepsilon_{inj} \sin(\omega_{inj}t)$. Detailed proof is provided in Appendix. Therefore, $v_S(t)$ includes components at both the fundamental harmonic (FH) of the switching frequency and

the injection (Inj) frequency f_{inj} . Therefore, there will also be components of $v(t)$ and $i_L(t)$ at frequencies of the f_s and the f_{inj} . In Fig. 2(b), the waveforms for Buck converters including “dc,” “dc + FH,” and “dc + FH + Inj” components are shown after injection. The f_s is typically much larger than the f_{inj} . One can observe that additional information, i.e., the “Inj” component, is brought to the parameter estimation problem.

C. Selection of Injection Frequencies and Transfer Functions

To achieve capacitance estimation, various measurements should be installed. Typical measurements for Buck converters include the output voltage $v(t)$ and the inductor current $i_L(t)$. With the equivalent source $v_S(t)$ generated by the injection, $v(t)$ and $i_L(t)$ also consist of dc, FH, and higher harmonic of f_s , and component at f_{inj} . In this article, the components at f_{inj} , i.e., $v_{inj}(t)$ and $i_{L,inj}(t)$, are the components of interest, and other components can be filtered out.

In s domain, from the physical laws of the circuit, the transfer function $V_{inj}(s)/V_{S,inj}(s)$ and $I_{L,inj}(s)/V_{S,inj}(s)$ are

$$V_{inj}(s)/V_{S,inj}(s) = G_2(s)/G_1(s) \quad (2)$$

$$I_{L,inj}(s)/V_{S,inj}(s) = G_3(s)/G_1(s) \quad (3)$$

where the s domain expressions $V_{inj}(s)$, $I_{L,inj}(s)$, and $V_{S,inj}(s)$ correspond to the time domain expressions $v_{inj}(t)$, $i_{L,inj}(t)$, and $v_{S,inj}(t)$, respectively. $G_1(s) = LC(R+R_C)s^2 + (L+CR(R_L+R_C) + CRR_C R_L)s + R + R_L$, $G_2(s) = R(CR_Cs + 1)$, $G_3(s) = C(R + R_C)s + 1$.

According to the derivation in Section II-B, the duty cycle injection $d_{inj}(t) = \varepsilon_{inj} \sin(\omega_{inj}t)$ will generate a component $v_{S,inj}(t) = V_g \varepsilon_{inj} \sin(\omega_{inj}t)$ in $v_S(t)$. Therefore, the transfer functions among $V_{inj}(s)$, $I_{L,inj}(s)$, and $D_{inj}(s)$ are

$$G_{vd}(s) = V_{inj}(s)/D_{inj}(s) = V_g G_2(s)/G_1(s) \quad (4)$$

$$G_{id}(s) = I_{L,inj}(s)/D_{inj}(s) = V_g G_3(s)/G_1(s) \quad (5)$$

$$G_{vi}(s) = V_{inj}(s)/I_{L,inj}(s) = G_2(s)/G_3(s). \quad (6)$$

Now, the transfer function $G(s)$, including three candidates $G_{vd}(s)$, $G_{id}(s)$, and $G_{vi}(s)$, can be used to estimate the parameter of the capacitance C . For the rest of the article, $G(s)$ is rewritten as $|G(C, s)|$ with the unknown variable C . At the injection angular frequency ω_{inj} , with $s = j\omega_{inj}$, $|G(C, j\omega_{inj})|$ (calculated from available measurements) only contains one unknown variable C . Therefore, the variable C can be solved.

1) *Selection of Injection Frequencies*: Ideally speaking, the capacitance C can be estimated with any user-selected injection angular frequency ω_{inj} . However, in practice, the error of the calculated $|G(C, j\omega_{inj})|$ (due to non-ideal measurements) will propagate to the estimated C . Therefore, the injection angular frequency ω_{inj} should be carefully designed to ensure minimum estimation error of C .

Here, the sensitivity of capacitance C is defined as the partial derivative of $|G(C, j\omega_{inj})|$ with respect to C , after normalization

$$S_G(C, \omega_{inj}) = \left| \frac{\partial |G(C, j\omega_{inj})| / |G(C, j\omega_{inj})|}{\partial C / C} \right|. \quad (7)$$

From (7), the accuracy of estimating C will vary with different injection angular frequency. Given the relative error of

the calculated $|G(C, j\omega_{inj})|$ as $\Delta|G(C, j\omega_{inj})|/|G(C, j\omega_{inj})|$, the relative error of the estimated capacitance is

$$\left| \frac{\Delta C}{C} \right| = \frac{|\Delta|G(C, j\omega_{inj})|/|G(C, j\omega_{inj})||}{S_G(C, \omega_{inj})}. \quad (8)$$

From (8), it can be seen that the sensitivity $S_G(C, \omega_{inj})$ is an important metric to evaluate the accuracy of capacitance estimation. If ω_{inj} is selected such that $S_G(C, \omega_{inj})$ is small, the estimation error of C will be large even with small errors of $|G(C, j\omega_{inj})|$. In practice, the relative errors of the transfer function $\Delta|G(C, j\omega_{inj})|/|G(C, j\omega_{inj})|$ are determined by the errors of various measurement devices. Here for simplicity, we assume that the values of $\Delta|G(C, j\omega_{inj})|/|G(C, j\omega_{inj})|$ for various transfer functions are similar. Therefore, to ensure minimized estimation error of C , $S_G(C, \omega_{inj})$ should reach maximum. In this case, ω_{inj} can be selected close to the characteristic angular frequency $\omega_{inj(chara)}$, and $f_{inj(chara)} = \omega_{inj(chara)}/2\pi$

$$\omega_{inj(chara)} = \underset{\omega_{inj}}{\operatorname{argmax}} S_G(C, \omega_{inj}). \quad (9)$$

To obtain $\omega_{inj(chara)}$, the necessary condition is

$$\partial S_G(C, \omega) / \partial \omega \Big|_{\omega=\omega_{inj(chara)}} = 0. \quad (10)$$

In Section II-B, this article assumes that $f_{inj} \ll f_s$ for the derivation. Therefore, after extracting $\omega_{inj(chara)}$ from (9), it is important to verify whether $\omega_{inj(chara)}$ is indeed much less than ω_s , to ensure that the derivation in Appendix still holds. Fortunately, the aforementioned assumption always holds with typical circuit and system parameters. Details can be found in Sections III and IV.

2) *Selection of Transfer Functions*: In fact, there are three candidate transfer functions (4)–(6) for capacitance estimation. From (10), three characteristic frequencies $\omega_{inj(chara),Gvd}$, $\omega_{inj(chara),Gid}$ and $\omega_{inj(chara),Gvi}$ can be calculated for three transfer functions, respectively. Substitute the three characteristic frequencies into (7) to obtain S_{Gvd} , S_{Gid} , and S_{Gvi} . Among three sensitivity values, the largest one corresponds to the selected transfer function, as follows:

$$G = \underset{G}{\operatorname{argmax}} S_G(G = G_{vd}, G_{id}, G_{vi}). \quad (11)$$

Based on (9) for selection of injection angular frequency $\omega_{inj(chara)}$ and (11) for selection of transfer function G , the minimized estimation error of C can be guaranteed with (8).

3) *Analytical Solutions of Capacitance*: With the selected injection angular frequency ω_{inj} and the selected transfer function $G(C, s)$, the capacitance can be analytically solved. Next, for three possible selected transfer functions, the analytical solutions are derived, respectively. Substitute $s = j\omega_{inj}$ into (4)–(6)

$$\begin{aligned} |G_{vd}(C, j\omega_{inj})| &= \frac{V_{inj}}{\varepsilon_{inj}} \\ &= \sqrt{\frac{V_g^2(b_1(\omega_{inj})C^2 + b_0(\omega_{inj}))}{a_2(\omega_{inj})C^2 + a_1(\omega_{inj})C + a_0(\omega_{inj})}} \end{aligned} \quad (12)$$

$$\begin{aligned} |G_{id}(C, j\omega_{inj})| &= \frac{I_{L,inj}}{\varepsilon_{inj}} \\ &= \sqrt{\frac{V_g^2(b_2(\omega_{inj})C^2 + 1)}{a_2(\omega_{inj})C^2 + a_1(\omega_{inj})C + a_0(\omega_{inj})}} \end{aligned} \quad (13)$$

TABLE III
THREE DIFFERENT GROUPS CIRCUIT PARAMETERS,
SIMULATION SETTING

Group	1	2	3
$C=C_{init}$	520 μ F	220 μ F	520 μ F
L	31 μ H	31 μ H	3mH

$$|G_{vi}(C, j\omega_{inj})| = \frac{V_{inj}}{I_{L,inj}} = \sqrt{\frac{b_1(\omega_{inj})C^2 + b_0(\omega_{inj})}{b_2(\omega_{inj})C^2 + 1}} \quad (14)$$

where V_{inj} and $I_{L,inj}$ are the amplitudes of $v_{inj}(t)$ and $i_{L,inj}(t)$, respectively. $a_0(\omega) = L^2\omega^2 + (R + R_L)^2$, $a_1(\omega) = -2LR^2\omega^2$, $a_2(\omega) = (L(R + R_C))^2\omega^4 + (R(R_L + R_C) + R_C R_L)^2\omega^2$; $b_0(\omega) = R^2$, $b_1(\omega) = R^2 R_C^2 \omega^2$, and $b_2(\omega) = (R + R_C)^2 \omega^2$.

According to (12)–(14), the capacitance C always satisfies a quadratic equation. The analytical solution of capacitance C are shown in (15)–(17), while the negative roots in (15)–(17) are neglected

$$C = \left[-a_1|G_{vd}|^2 \pm \sqrt{\Delta_1} \right] / \left[2(a_2|G_{vd}|^2 - b_1V_g^2) \right] \quad (15)$$

$$C = \left[-a_1|G_{id}|^2 \pm \sqrt{\Delta_2} \right] / \left[2(a_2|G_{id}|^2 - b_2V_g^2) \right] \quad (16)$$

$$C = \sqrt{(b_0 - |G_{vi}|^2) / (b_2|G_{vi}|^2 - b_1)} \quad (17)$$

where $\Delta_1 = a_1^2|G_{vd}|^4 - 4(a_2|G_{vd}|^2 - b_1V_g^2)(a_0|G_{vd}|^2 - V_g^2)$, $\Delta_2 = a_1^2|G_{id}|^4 - 4(a_2|G_{id}|^2 - b_2V_g^2)(a_0|G_{id}|^2 - V_g^2)$. Here, the values of Δ_1 and Δ_2 are positive with typical parameters of a Buck circuit. The results in Sections III and IV also verify that the values of Δ_1 and Δ_2 are positive.

4) *Initial Value of Capacitance C_{init}* : From (7), (9), and (10), one can observe that $\omega_{inj(chara)}$ is a function of the capacitance C . In practice, due to aging procedure, the actual value of the capacitance C could deviate from the initial value of the capacitance C_{init} , with typical difference of less than 20% before the end of life of the capacitor [5], [6], [7]. Therefore, $\omega_{inj(chara)}$ can be approximated by substituting $C = C_{init}$ based on (9), and the selection of G for optimal sensitivity can also be chosen based on (11). With (15)–(17), the actual capacitance C can be estimated.

5) *Summary of Proposed Method*: To sum up, this part introduces the method based on the optimal sensitivity for accurate capacitance estimation. First, for estimation of aging capacitors, the initial value of the capacitance C_{init} should be given. Then, the optimal selection of injection frequencies and transfer functions is given based on known C_{init} . Finally, the actual capacitance C during the aging process can be directly estimated with analytical expressions based on the above selection.

The flowchart of proposed method is shown in Fig. 3.

III. SIMULATION RESULTS

To verify the proposed capacitance estimation method for Buck converters, the example test system in Fig. 1(a) is built in MATLAB/SIMULINK. Here, three possible Buck converter systems (Group 1 to 3) with various combinations of L and C are shown in Table III. For Group 1, capacitance $C = C_{init} = 520 \mu\text{F}$, inductance $L = 31 \mu\text{H}$, and other circuit parameters are shown in Table I. For Group 2 and Group 3, they only differ in choice of inductance and capacitance

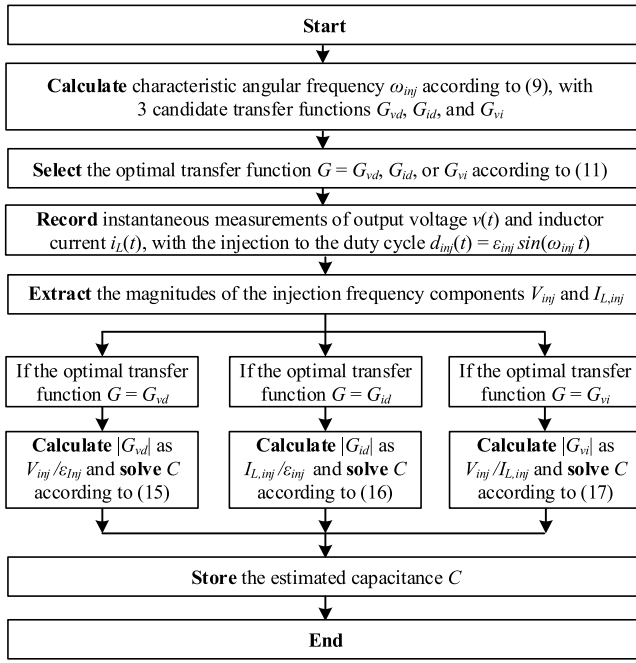


Fig. 3. Flowchart of the proposed method.

from Group 1. For all the three groups, the amplitude of duty cycle injection is selected as $\varepsilon_{inj} = 0.02$, satisfying $\varepsilon_{inj} \ll D = 0.5$. Note that the constant duty cycle D is set to be 0.5 as an example. The performances of the proposed method with other values of D are similar.

A. Results of Group 1

1) *Verification of Characteristic Injection Frequency for Optimal Sensitivity*: To verify that the optimal sensitivity is achieved at the characteristic injection frequency, for each transfer function G_{vd} , G_{id} , and G_{vi} , the values of $|G(C, j\omega)|$ and $S_G(C, j\omega)$ as functions of capacitance and frequency are depicted in Fig. 4.

According to Section II, the characteristic injection frequency is calculated given the capacitance $C = C_{init} = 520 \mu\text{F}$. To begin with, for the transfer function G_{vd} , the value of $|G_{vd}|$ in Fig. 4(a) reaches maximum rate of change at around 500 Hz. The sensitivity results $S_{G_{vd}}$ shown in Fig. 4(b) confirms that the optimal sensitivity is achieved at $f_{inj} = 523$ Hz. The black solid circle is the point of optimal sensitivity corresponding to the characteristic injection frequency $f_{inj(char)}$ (marked as the red pentagram). However, even if the characteristic frequency signal is injected, the value of the optimal sensitivity is still relatively low ($S_{G_{vd}} = 0.195$). According to the analysis in (8), it can be concluded that the error of the estimated capacitance will become $1/S_{G_{vd}} \approx 5$ times of the error of the measurement.

Similarly, if the other two transfer functions G_{id} and G_{vi} are taken into consideration given the same capacitance $C = C_{init}$, the sensitivities $S_{G_{id}}$ and $S_{G_{vi}}$ reaches maximum at $f_{inj} = 121$ Hz and $f_{inj} = 143$ Hz in Fig. 4(d) and (f), respectively. The optimal sensitivities are $S_{G_{id}} = 0.803$ and $S_{G_{vi}} = 0.854$. One can observe that $S_{G_{vi}} = 0.854$ is more than 4 times of $S_{G_{vd}} = 0.195$. According to Section II, the transfer function is selected as $G = G_{vi}$ for Group 1 circuit parameter estimation. The above results are summarized in Table IV.

TABLE IV

SUMMARY OF CHARACTERISTIC INJECTION FREQUENCY, MODULUS AND OPTIMAL SENSITIVITY FOR GROUP 1 SETTINGS, SIMULATION

Transfer Functions	G_{vd}	G_{id}	G_{vi}
$f_{inj(char)}/\text{Hz}$	523	121	143
$ G(C_{init}, \omega_{inj(char)}) $	4.07	2.08	1.97
$\max S_G(C_{init}, \omega_{inj(char)})$	0.195	0.803	0.854

2) *Verification of Characteristic Frequency for Minimum Capacitance Estimation Error*: According to Section III-A1, the characteristic injection frequency with the selected transfer function can achieve optimal sensitivity. To verify the necessity of above selection, the capacitance estimation errors with various candidate transfer functions and injection frequencies are demonstrated below. In this section, the capacitance value is assumed to be the nominal value, i.e., $C = C_{init}$.

Throughout the simulation, the Buck converter operates with 11 different injection frequencies ($f_{inj} = 50, 100, 200, 300, 400, 500, 600, 700, 800, 900,$ and 1000 Hz), respectively. The measurements are recorded and the values of $|G_{vd}|$, $|G_{id}|$, and $|G_{vi}|$ are calculated. Next, the 1% errors are superimposed on the values of $|G_{vd}|$, $|G_{id}|$, and $|G_{vi}|$ (i.e., $\Delta|G(C, j\omega)|/|G(C, j\omega)| = 1\%$). The circles in Fig. 5 show the measured 33 values of $|G|$, with three different transfer functions ($G = G_{vd}$, G_{id} , and G_{vi}) and 11 different injection frequencies. In each sub-figure, the solid circle represents the frequency with maximum sensitivity among the 11 different frequencies (the definitions of solid circles are the same for the rest of the article). Note that the maximum slope of $|G|$ in Fig. 5 does not correspond to the maximum sensitivity, as the sensitivity is defined as the $|\partial|G|/\partial C \cdot C/G|$.

With the measurements in Fig. 5, the capacitance can be solved with different injection frequencies, as shown in Fig. 6. Specifically, in Fig. 6(a), one can observe that, for each transfer function ($G = G_{vd}$, G_{id} , and G_{vi}), the minimum capacitance estimation errors are achieved with the injection frequency $f_{inj} = 500$ Hz, $f_{inj} = 100$ Hz, and $f_{inj} = 200$ Hz, respectively. Those injection frequencies are close to the calculated characteristic frequencies in Table IV for each transfer function. Among them, the minimum error is achieved with the injection frequency 200 Hz and the transfer function G_{vi} . Also, the capacitance estimation error will greatly increase if the injection frequency is far away from the characteristic frequency. These results are consistent with the sensitivity results in Fig. 6(b): the maximum sensitivity corresponds to the minimum capacitance estimation error.

3) *Capacitance Estimation Results During Capacitance Attenuation With Characteristic Frequency Injection*: To simulate the process of capacitance attenuation during aging of aluminum electrolytic capacitors, three capacitors with different capacitance values were selected, namely $520 \mu\text{F}$ (Cap1: 100% of C_{init}), $468 \mu\text{F}$ (Cap2: 90% of C_{init}), and $416 \mu\text{F}$ (Cap3: 80% of C_{init}). Since one does not know the actual values of capacitance before the estimation procedure, for simplicity, the characteristic injection frequencies are calculated identically for these three different capacitances Cap1–Cap3, all with $C = C_{init}$ (nominal value). Therefore, the choice of characteristic injection frequency is same as that shown in Table IV, i.e., $f_{inj} = 523, 121,$ and 143 Hz, for transfer functions $G = G_{vd}$, G_{id} , and G_{vi} , respectively.

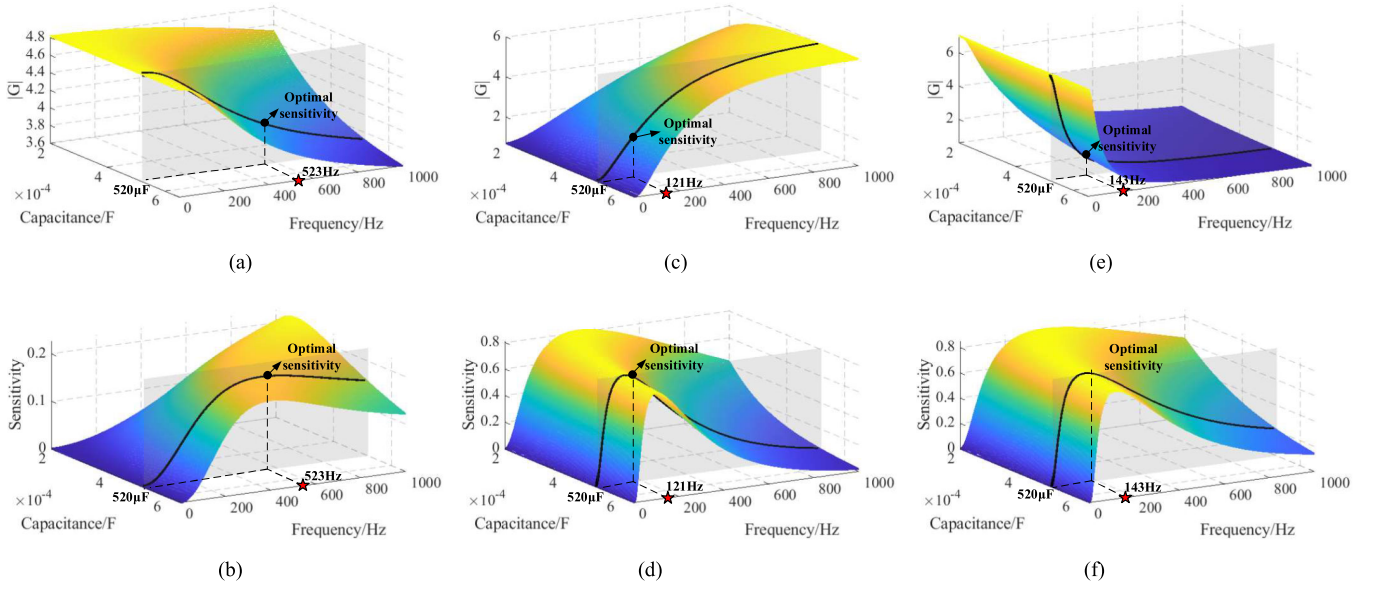


Fig. 4. Values of $|G|$ and S_G as functions of capacitance and frequency, three different transfer functions, Group 1. (a) $|G_{vd}|$. (b) $S_{G_{vd}}$. (c) $|G_{id}|$. (d) $S_{G_{id}}$. (e) $|G_{vi}|$. (f) $S_{G_{vi}}$.

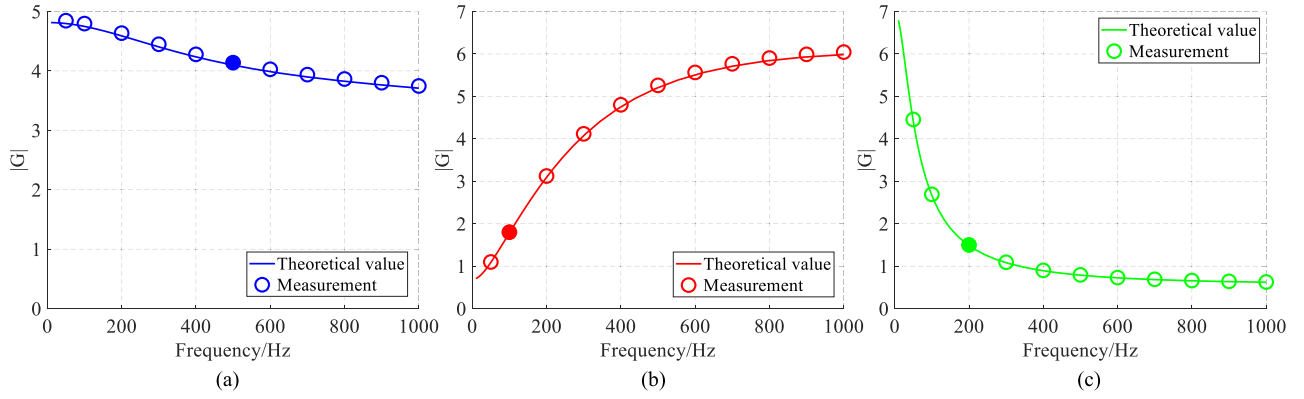


Fig. 5. Values of $|G|$ with different injection frequencies, three different transfer functions, Group 1, simulation. (a) $|G_{vd}|$. (b) $|G_{id}|$. (c) $|G_{vi}|$.

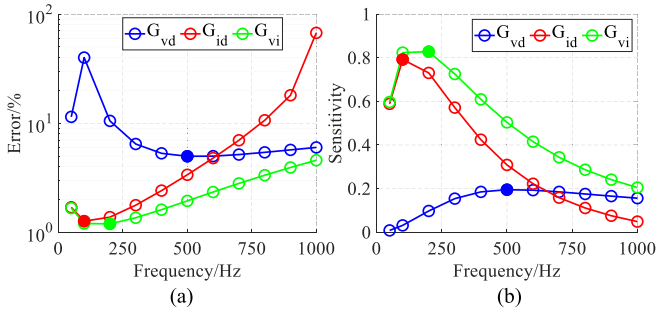


Fig. 6. Capacitance estimation error and sensitivity for different injection frequencies using three transfer functions, Group 1, simulation. (a) Capacitance estimation error. (b) Sensitivity.

With the injection frequency at the characteristic frequency, the capacitance estimation results are provided. Here, similar as Section III-A2, the 1% fixed deviation is superimposed on the values of $|G_{vd}|$, $|G_{id}|$, and $|G_{vi}|$ as the noise source for the simulation. The capacitance estimation error and sensitivity using the transfer functions G_{vd} , G_{id} , and G_{vi} are shown in Table V. The capacitance estimation errors vary from

1.16% to 1.18% for G_{vi} , while the errors vary from 1.25% to 1.27% for G_{id} and from 4.96% to 5.10% for G_{vd} . The results prove that the choice of G_{vi} with characteristic frequency injection corresponds to high parameter sensitivity and low capacitance estimation error, even when the capacitance attenuation reaches 20%. This shows the proposed method can accurately estimate values of capacitance and mark the end of life of capacitors.

B. Results of Group 2

1) *Verification of Characteristic Injection Frequency for Optimal Sensitivity:* Next, the characteristic injection frequency for optimal sensitivity is similarly verified for Group 2. The initial capacitance C_{init} in Group 2 is updated from 520 to 220 μF compared to that in Group 1, as shown in Table III. For three candidate transfer functions, the calculated characteristic injection frequency and the function values of at the characteristic injection frequency are summarized in Table VI. Similarly, the selected transfer function G_{vi} corresponds to the maximum sensitivity ($S_{G_{vi}} = 0.854$) at its characteristic frequency [$f_{inj(char)} = 339 \text{ Hz}$].

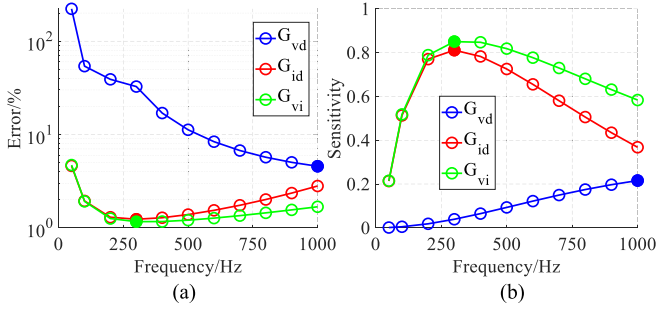


Fig. 7. Capacitance estimation error and sensitivity for different injection frequencies using three transfer functions, Group 2, simulation. (a) Capacitance estimation error. (b) Sensitivity.

TABLE V

CAPACITANCE ESTIMATION ERROR AND SENSITIVITY, INJECTION AT CHARACTERISTIC FREQUENCIES, GROUP 1, SIMULATION

Error of Estimation	G_{vd}	G_{id}	G_{vi}
Cap1	4.96%	1.25%	1.16%
Cap2	4.96%	1.25%	1.16%
Cap3	5.10%	1.27%	1.18%
Sensitivity	G_{vd}	G_{id}	G_{vi}
Cap1	0.195	0.803	0.854
Cap2	0.196	0.800	0.851
Cap3	0.192	0.790	0.842

2) *Verification of Characteristic Frequency for Minimum Capacitance Estimation Error:* Similar as the settings of Group 1 in Section III-A2, 11 various injection frequencies from 50 Hz to 1 kHz are studied. For each injection frequency, the output voltage and inductor current measurements are extracted, and 1% measurement errors are superimposed. The capacitance estimation results for 11 injection frequencies and 3 transfer functions are shown in Fig. 7(a). Similarly, the capacitance estimation errors are minimized when the injection frequencies are selected close to the characteristic frequencies, for all three candidate transfer functions. The sensitivity results shown in Fig. 7(b) also indicate that higher sensitivity corresponds to lower capacitance estimation error. The results also prove the selection of transfer function G_{vi} can guarantee maximum sensitivity and minimum estimation error.

3) *Capacitance Estimation Results During Capacitance Attenuation With Characteristic Frequency Injection:* Here, three capacitors with different capacitance values were selected to reflect the capacitance attenuation process: 220 μF (Cap 1: 100% of C_{init}), 198 μF (Cap 2: 90% of C_{init}), and 176 μF (Cap 3: 80% of C_{init}). With the injection frequency at the characteristic frequency 339 Hz, the capacitance estimation error and sensitivity using the transfer functions G_{vd} , G_{id} , and G_{vi} are shown in Table V. The capacitance estimation errors vary from 1.16% to 1.18% for G_{vi} , while the errors vary from 1.23% to 1.25% for G_{id} and from 3.30% to 3.59% for G_{vd} . The results prove that the choice of G_{vi} with characteristic frequency injection corresponds to high parameter sensitivity and low capacitance estimation error.

Finally, for the comparison between Tables V and VII, if the value of capacitance is updated from 520 to 220 μF , the characteristic injection frequency should also be updated

TABLE VI

SUMMARY OF CHARACTERISTIC INJECTION FREQUENCY, MODULUS AND OPTIMAL SENSITIVITY FOR GROUP 2 SETTINGS, SIMULATION

TFs	G_{vd}	G_{id}	G_{vi}
$f_{inj(char)}/\text{Hz}$	1740	293	339
$ G(C_{init}, \omega_{inj(char)}) $	3.99	2.14	1.97
$\max S_G(C_{init}, \omega_{inj(char)})$	0.270	0.811	0.854

TABLE VII

SENSITIVITY AND CAPACITANCE ESTIMATION ERROR, INJECTION AT CHARACTERISTIC FREQUENCIES, GROUP 2, SIMULATION

Error of Capacitance	G_{vd}	G_{id}	G_{vi}
Cap1	3.59%	1.23%	1.16%
Cap2	3.41%	1.24%	1.16%
Cap3	3.30%	1.25%	1.18%
Sensitivity	G_{vd}	G_{id}	G_{vi}
Cap1	0.270	0.811	0.854
Cap2	0.285	0.810	0.851
Cap3	0.296	0.799	0.842

TABLE VIII

SUMMARY OF CHARACTERISTIC INJECTION FREQUENCY, MODULUS AND OPTIMAL SENSITIVITY FOR GROUP 3 SETTINGS, SIMULATION

TFs	G_{vd}	G_{id}	G_{vi}
$f_{inj(char)}/\text{Hz}$	174	90	143
$ G(C_{init}, \omega_{inj(char)}) $	3.79	2.45	1.97
$\max S_G(C_{init}, \omega_{inj(char)})$	1.19	1.11	0.854

from 143 to 339 Hz, to ensure maximum sensitivity and minimum estimation error. Also, if the injection frequency is still 143 Hz for the 220 μF system in Group 2, the capacitance estimation error will increase from 1.16%~1.18% to 1.46%~1.71%. This also proves the importance to adjust injection frequency according to the parameters of the system.

C. Results of Group 3

1) *Verification of Characteristic Injection Frequency for Optimal Sensitivity:* The characteristic injection frequency for optimal sensitivity is similarly verified for Group 3. The inductance L is increased from 330 μH in Group 1 to 3 mH in Group 3, as shown in Table III. The characteristic injection frequency and maximum sensitivity value are included in Table VIII. One can observe that the selected transfer function G_{vd} corresponds to the maximum sensitivity ($S_{G_{vd}} = 1.19$) at its characteristic frequency [$f_{inj(char)} = 174$ Hz].

2) *Verification of Characteristic Frequency for Minimum Capacitance Estimation Error:* For this part, the simulation experiment is similar to the settings of Group 1 in Section III-B2. The 11 injection frequencies from 50 Hz to 1 kHz are chosen, and 1% measurement errors are superimposed. In Fig. 8, the results prove that the choice of function G_{vd} can guarantee maximum sensitivity and minimum estimation error of capacitance.

3) *Capacitance Estimation Results During Capacitance Attenuation With Characteristic Frequency Injection:* Same as the Group 1 setting, three capacitors with different capacitance values were selected as 520 μF (Cap1: 100% of C_{init}), 468 μF (Cap2: 90% of C_{init}), and 416 μF (Cap3: 80% of C_{init}).

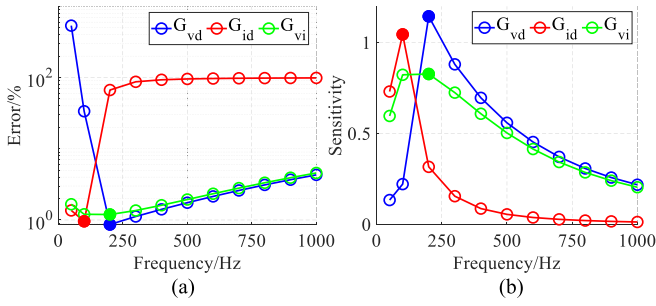


Fig. 8. Capacitance estimation error and sensitivity for different injection frequencies using three transfer functions, Group 3, simulation. (a) Capacitance estimation error. (b) Sensitivity.

TABLE IX

SENSITIVITY AND CAPACITANCE ESTIMATION ERROR, INJECTION AT CHARACTERISTIC FREQUENCIES, GROUP 3, SIMULATION

Error of Capacitance	G_{vd}	G_{id}	G_{vi}
Cap1	0.833%	0.904%	1.16%
Cap2	0.846%	0.915%	1.16%
Cap3	0.897%	0.949%	1.18%
Sensitivity	G_{vd}	G_{id}	G_{vi}
Cap1	1.19	1.11	0.854
Cap2	1.17	1.09	0.851
Cap3	1.11	1.05	0.842

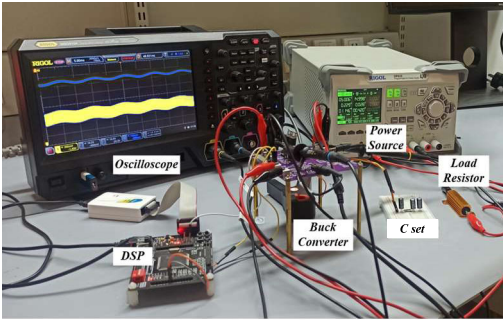


Fig. 9. Hardware experimental platform.

The capacitance estimation error and sensitivity results using the transfer functions G_{vd} , G_{id} , and G_{vi} are shown in Table IX. The capacitance estimation errors vary from 0.833% to 0.897% for G_{vd} , while the errors vary from 0.904% to 0.949% for G_{id} and from 1.16% to 1.18% for G_{vi} . The results prove that the choice of G_{vd} with characteristic frequency injection corresponds to high parameter sensitivity and low capacitance estimation error. In summary, three different groups of parameter settings discuss the verification of characteristic injection frequency, relationship between the estimation error and sensitivity, and capacitance estimation during capacitance attenuation. Group 2 differs from Group 1 in that the initial capacitance value C_{init} is reduced, and the transfer function G_{vi} is still the best candidate equation. Then, for the Group 3 parameter setting (only the change of inductance compared to that in Group 1), G_{vd} becomes the selected transfer function with the optimal sensitivity and minimum error.

IV. HARDWARE EXPERIMENTAL RESULTS

In this section, the hardware experiments are conducted to further ensure the effectiveness of the proposed capacitance parameter estimation method. Fig. 9 shows the hardware

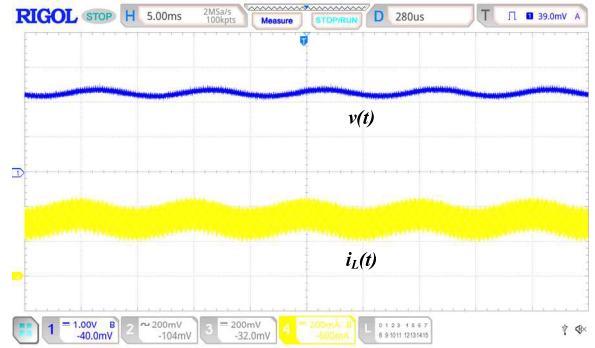


Fig. 10. Waveforms of output voltage $v(t)$ and inductor current $i_L(t)$ with 100 Hz injection frequency, hardware experiments.

experimental platform. The topology of the Buck converter is the same as that in Fig. 1. The input of the Buck converter is provided by the power source (Rigol, DP832), while the load is a resistor. The states of switches are controlled by the DSP (Texas Instrument, TMS320F28335), and the injection to the duty cycle is also implemented by the DSP. The constant duty cycle $D = 0.5$, and the amplitude of the duty cycle injection is $\varepsilon_{inj} = 0.02 \ll D$. The output voltage and inductor current are sampled using the oscilloscope (Rigol, MSO5104). The initial capacitance C_{init} in this circuit is $520 \mu\text{F}$. The “C set” in the figure is adopted to conveniently update the value of the capacitance, in order to mimic the capacitance attenuation during the aging procedure. The “C set” includes three capacitors: $520 \mu\text{F}$ (Cap1: 100% of C_{init}), $460 \mu\text{F}$ (Cap2: 90% of C_{init}), and $418 \mu\text{F}$ (Cap3: 80% of C_{init}). The system parameters are the same as those of Group 1 in Section III-A. With the proposed method, the characteristic injection frequencies for different candidate transfer functions are calculated and the results are the same as those in Table IV.

Similar as the setup in Section III-A (Group 1), different injection frequencies are selected as 50, 100, 200, 300, 400, 500, 600, 700, 800, 900, and 1000 Hz. Fig. 10 shows an example of measured output voltage $v(t)$ and inductor current $i_L(t)$, where the injection frequency is set as 100 Hz. The output waveforms contain “dc” component, “FH” (of the switching frequency), and the injection frequency, which is consistent with the results of theoretical analysis in Section II-A. One can observe that the injection does not affect the normal operation of the converter due to small perturbation on duty cycle. To obtain the injection frequency component for capacitance estimation, the dc component is first filtered out by setting the sampling channel of the oscilloscope to be ac-coupled. Then, the harmonics of the switching frequency are filtered out by a second-order Butterworth digital low-pass filter with the cutoff frequency of 5 kHz. After filtering, the waveforms only contain the components at the injection frequency ($v_{inj}(t)$), the amplitude of which is V_{inj} .

For the experiments above, the capacitance estimation results when solving capacitance $C = C_{init}$ with three different transfer functions as candidate equations are tested, respectively. The measurement $|G|$ values of hardware experiments are shown in Fig. 11. The capacitance estimation error results are shown in Fig. 12. One can observe that three transfer functions G_{vd} , G_{id} , and G_{vi} achieve the smallest capacitance estimation error in 500, 100, and 200 Hz, respectively

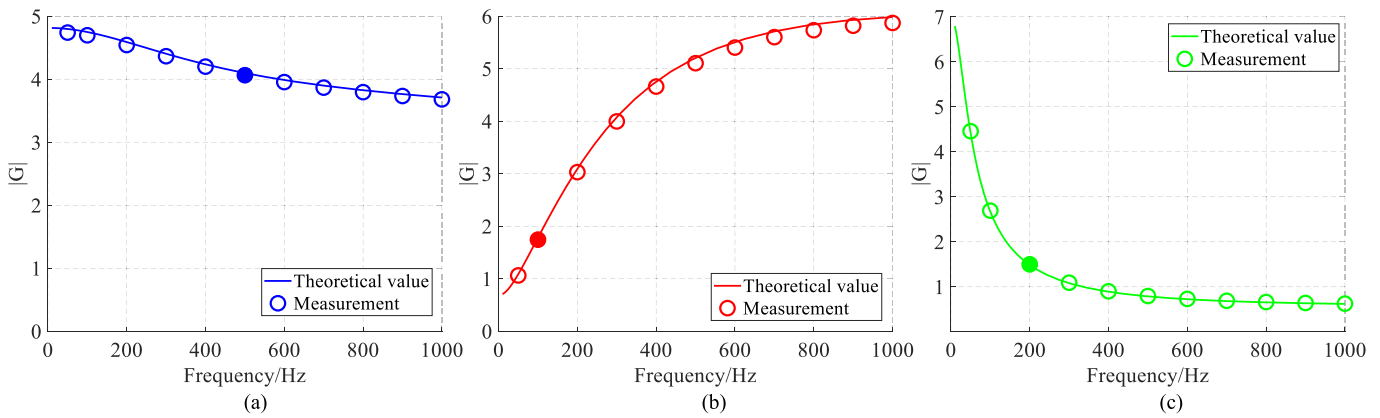


Fig. 11. Values of $|G|$ with different injection frequencies, three different transfer functions, and hardware experiments. (a) $|G_{vd}|$. (b) $|G_{id}|$. (c) $|G_{vi}|$.

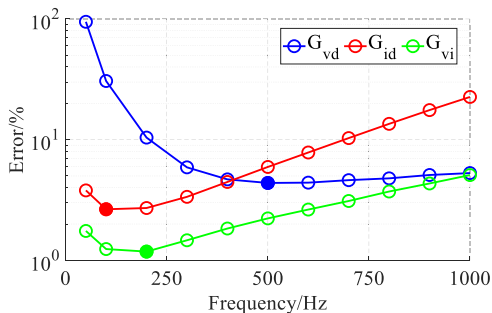


Fig. 12. Capacitance estimation error for different injection frequencies using three transfer functions, Group 1, hardware experiments.

TABLE X

CAPACITANCE ESTIMATION ERROR, INJECTION AT CHARACTERISTIC FREQUENCIES, HARDWARE EXPERIMENTS

Error of Capacitance	G_{vd}	G_{id}	G_{vi}
Cap1	5.31%	2.49%	1.18%
Cap2	5.25%	2.50%	1.19%
Cap3	5.34%	2.53%	1.20%

(marked as solid circles). Among them, the capacitance estimation error using the selected transfer function G_{vi} is smallest compared to that using transfer functions G_{vd} and G_{id} . The optimal selection of injection frequency for G_{vi} is close to the 200 Hz.

Similar as Section III-A, three capacitors with different capacitance values were selected, namely 520 μF (Cap1: 100% of C_{init}), 460 μF (Cap2: about 90% of C_{init}), and 418 μF (Cap3: about 80% of C_{init}). The characteristic injection frequency is selected according to the initial value of the capacitance C_{init} , i.e., 523 Hz (for G_{vd}), 121 Hz (for G_{id}), and 143 Hz (for G_{vi}), respectively. Waveforms of output voltage and inductor current with different capacitances at characteristic injection frequencies are shown in Fig. 13, respectively. In Fig. 13, the dc components of those waveforms have been filtered out using ac-coupled sampling channel on the oscilloscope. The blue curve represents the output voltage while the yellow curve represents the inductor current without the dc offset.

The estimation results using above three transfer functions G_{vd} , G_{id} , and G_{vi} are shown in Table X. With the

characteristic injection frequency, selected transfer function G_{vi} can result in capacitance estimation errors less than 1.20%. In comparison, the errors of capacitance estimation for G_{vd} and G_{id} are 5.25%~5.34% and 2.49%~2.53%. The hardware experimental results further prove the necessity to select the proper transfer function and to inject at the characteristic frequency for optimal parameter sensitivity.

V. DISCUSSION

A. Comparison to Different Existing Methods

In this section, more comparisons between the proposed method and the existing methods are provided.

First, ripple-based methods [9], [10], [11], [12] are based on circuit responses at the switching frequency to estimate capacitance. According to the analysis in Section II-A, these methods will encounter sensitivity issues when estimating capacitances, limiting their capacitance estimation accuracy.

Second, the abrupt change-based methods [13], [14], [15], [16], [17] require specific operating conditions of the system (e.g., abrupt change from load 1 to load 2, circuit start-up, change of circuit topology) to generate additional information about circuit dynamics. Therefore, these methods could be limited when the system operating conditions are not allowed to be changed. In addition, these methods typically require dynamic time domain model consisting of differential equations, which could be complicated in practice.

Third, the injection-based methods [18], [19], [20], [21], [22] generate additional information by injecting various frequencies into the circuit. Wideband injection-based methods [18], [19], [20] usually inject frequencies within a wide range. However, these methods are still based on complicated dynamic time domain model. Existing single-frequency injection-based methods select injection frequency empirically [21] or based on other objectives such as THD [22]. These selections do not minimize the capacitance estimation error. As a result, the capacitance estimation error could also be increased. This fact is also verified via hardware experiments as shown in Fig. 12, where the estimation errors are increased with injection frequency away from the characteristic frequency proposed in this article.

The proposed method belongs to the group of single-frequency injection-based methods. Compared to the ripple-based method, the proposed method has higher

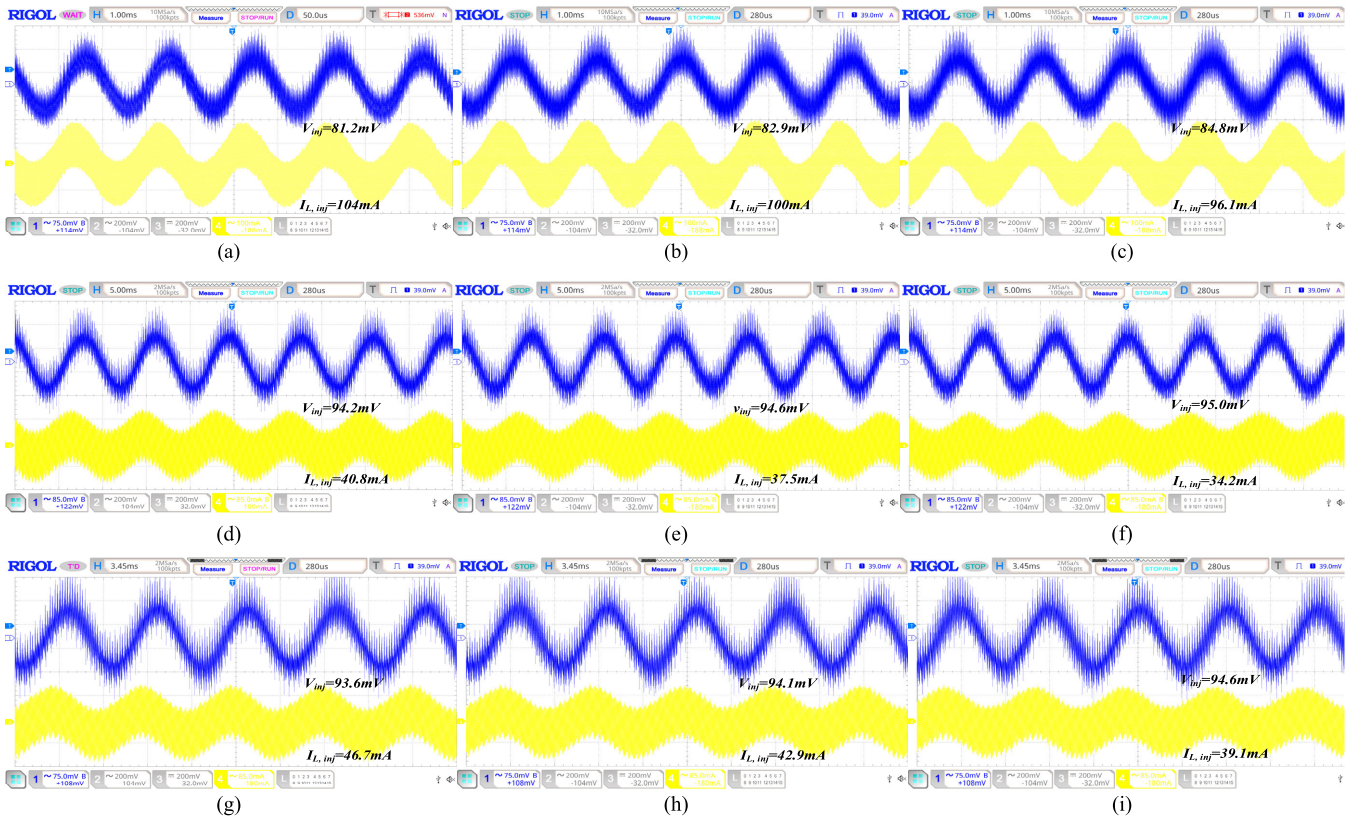


Fig. 13. Injection output voltage and inductor current waveforms at the characteristic injection frequency for three different transfer functions and capacitors from Cap1 to Cap3, hardware experiments. Row 1: (a) Cap1, 523 Hz. (b) Cap2, 523 Hz. (c) Cap3, 523 Hz. Row 2: (d) Cap1, 121 Hz. (e) Cap2, 121 Hz. (f) Cap3, 121 Hz. Row 3: (g) Cap1, 143Hz. (h) Cap2, 143 Hz. (i) Cap3, 143 Hz.

estimation accuracy. Compared to the abrupt change-based method, the proposed method does not need specific operating condition, and does not need dynamic time domain model. Compared to wideband injection-based method, the proposed method does not need dynamic time domain model, and the estimation procedure is much simplified. Compared to existing single-frequency injection-based methods, the proposed method selects transfer function and injection frequency with optimal sensitivity, to ensure smaller capacitance estimation error.

To sum up, the comparison between the proposed method and the existing methods is shown in detail in Table XI.

B. Influence of Different Measurement Devices on Capacitance Estimation Errors

From (8) in Section II-C, selecting the injection frequency and transfer function with maximum sensitivity can ensure minimum capacitance estimation error. However, one important assumption is that the values of $|\Delta G/G|$ for the three transfer functions G_{vd} , G_{id} , and G_{vi} are similar. These values are determined by measurement errors of output voltage $v(t)$ and inductor current $i_L(t)$.

To verify whether the above assumption is true, the values of $|\Delta G/G|$ for the three transfer functions G_{vd} , G_{id} , and G_{vi} during the hardware experiments in Section IV are depicted in Fig. 14. One can observe that the orders of magnitudes of $|\Delta G/G|$ for three transfer functions are indeed similar. However, the value of $|\Delta G_{id}/G_{id}|$ is a little larger than

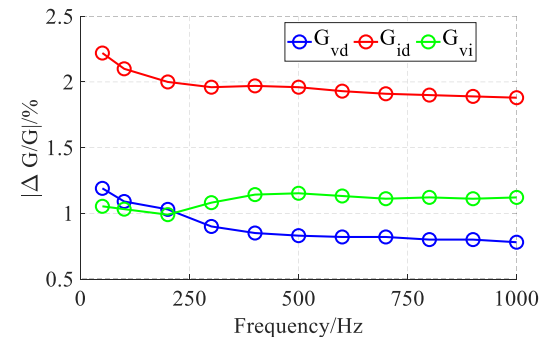


Fig. 14. $|\Delta G/G|$ for different injection frequency using three transfer functions, Group 1, hardware experiments.

the values of $|\Delta G_{vd}/G_{vd}|$ and $|\Delta G_{vi}/G_{vi}|$. This is probably because the errors of current measurements are higher than those of voltage measurements, which is a typical scenario in practice.

In practice, more factors could be considered to improve the proposed capacitance estimation method. First, the errors of measurement devices can also be taken into account. With given measurement errors, from (8), the transfer function and injection frequency can be selected according to the ratio between parameter sensitivity and measurement error. Second, one should also consider the cost/compactness of measurement devices as well as the impact of installing the measurement devices on the original circuit, to ensure practicability of the proposed method.

TABLE XI
COMPARISON TO DIFFERENT EXISTING METHODS

Methods	Refs	Power converter	Additional information?	No need for specific operating condition?	No need for dynamic time domain model?	Selection of injection frequency to minimize estimation error?	Capacitance estimation accuracy
Ripple based methods	[9-12]	Boost/PFC/AC-DC-AC PWM	×	✓	✓	N. A	+
Abrupt change based methods	[13-17]	Buck/Boost/AC-DC-AC PWM	✓ (circuit dynamics)	× (e.g., load change)	× (e.g., state space model)	N. A	+++
Injection based methods	[18-20]	Buck	✓ (wide frequency range)	✓	× (e.g., auto regressive model)	N. A	+++
	[21]	Buck	✓ (single frequency)	✓	✓	× (empirical selection)	++
	[22]	AC-DC-AC PWM	✓ (single frequency)	✓	✓	× (minimizing THD)	++
	Proposed method	Buck	✓ (single frequency)	✓	✓	✓ (optimal sensitivity)	+++

Notes: Ref (References); N. A (Not Applicable); more “+” means higher accuracy.

C. Calculation of Other Parameters in the Buck Circuit

In Section II-C, the proposed method calculates the capacitance based on (15)–(17). In these equations, the coefficients $a_0, a_1, a_2, b_0, b_1,$ and b_2 are functions of the circuit parameters, including L (the inductance of the inductor), R_L (resistance of the inductor), R (the load resistance), and R_C (the ESR of the capacitor). Availability of these parameters will affect the effectiveness of the proposed method.

In practice, there are two ways to obtain these parameters. The first way is to directly measure them offline before the capacitance estimation procedure. However, the values of the parameters could deviate from their nominal values during operation of the circuit. For example, the ESR could also change during the aging procedure of the capacitor. The second way is to estimate them online using the physical laws of the circuit. The value of R_L can be calculated as $(DV_g - V)/I_L$, according to the dc equivalent circuit in Fig. 1(c). The value of L can be calculated as $[v_S(t) - v(t) - R_L i_L(t)]/[di_L(t)/dt]$, according to the circuit in Fig. 1(b). This expression can be further simplified with small ripple approximation [23]. The value of R can be calculated as V/I_L , according to the dc equivalent circuit in Fig. 1(c). One typical method for estimation of R_C is $R_C = \Delta v/\Delta i_L$ [11], where Δv and Δi_L are the ripple values of $v(t)$ and $i_L(t)$, respectively.

D. Other Discussions

1) *Application to Series and Parallel Electrolytic Capacitors:* The method proposed in this article considers the “capacitor unit” as one circuit element. In practice, the “capacitor unit” may include several electrolytic capacitors in series and/or in parallel. In this case, the proposed method can first identify whether the overall capacitance of the “capacitor unit” deviates from its nominal value. If the deviation is observed, the next step is to identify the specific degraded capacitors inside the “capacitor unit.” Additional measurements of voltages and currents inside the “capacitor unit” may be required to locate the exact degraded capacitors. Here, similar as

the proposed method in this article, active injection-based methods with optimal sensitivity could be adopted for capacitance estimation for series and/or parallel electrolytic capacitors.

2) *Application to High-Voltage Level:* In this article, the input voltage level of the Buck converter is set as 5 V to demonstrate the performance of the proposed capacitance estimation method. Here the electrolytic capacitor of interest has low voltage tolerance. If the electrolytic capacitor of interest has high-voltage tolerance, one should use a Buck circuit with high-voltage input, to ensure the operating environment as well as the degradation of the capacitor is practical.

3) *Application to Other Topologies:* The proposed method gives the sensitivity analysis for transfer functions in Buck converters, to provide guidance on selection of injection frequency and transfer functions for optimal sensitivity. This methodology can be potentially applied to parameter estimation problem in PWM converters with other topologies, where the injection frequency and transfer functions can be similarly selected according to the sensitivity analysis. These could be studied in future publications.

VI. CONCLUSION

This article proposes an online capacitance monitoring method for Buck converters based on characteristic frequency injection. The method actively selects the injection frequency and the transfer function for optimal parameter sensitivity. First, the relationship between the capacitance and the measurements is established by observing physical laws of system at the injection frequency. Next, the characteristic frequency is derived based on the optimal parameter sensitivity. The article provides clear guidance on the selection of the injection frequency with rigorous mathematical derivations: the injection frequency should be equal to the characteristic frequency to minimize the capacitance estimation error. The characteristic frequency and the parameter sensitivity for different transfer functions are studied, and the transfer function with the highest parameter sensitivity is selected for capacitance estimation

to further ensure estimation accuracy. Finally, simulation and hardware experiments prove that the optimal sensitivity can be achieved with characteristic frequency injection, and the proposed method presents accurate capacitance estimation results during aging of capacitors.

APPENDIX

Statement: With the duty cycle $d(t) = D + d_{inj}(t)$ where $d_{inj}(t) = \varepsilon_{inj} \sin(\omega_{inj}t)$, $\varepsilon_{inj} \ll D$ and $f_{inj} \ll f_s$, $v_S(t)$ should be equal to $DV_g + \sum_{k=1}^{\infty} V_g/(k\pi) \cdot (1 - \cos(2\pi kD)) \sin(k\omega_s t) + v_{S,inj}(t)$, where $v_{S,inj}(t) = V_g \varepsilon_{inj} \sin(\omega_{inj}t)$.

Proof: Before the injection to the duty cycle, with the constant duty cycle D , $v_S(t)$ is

$$v_S(t) = \begin{cases} V_g, & nT_s \leq t \leq (n+D)T_s \\ 0, & (n+D)T_s \leq t \leq (n+1)T_s \end{cases} \quad (\text{A-1})$$

where T_s is switching period and n represents the n th period.

After the injection to the duty cycle, $d(t) = D + d_{inj}(t)$. Since $f_{inj} \ll f_s$, it can be assumed that $f_s \approx Nf_{inj}$, where $N \gg 1$ is a large integer. In this case, the injection period T_{inj} is much larger than the switching period T_s ($T_{inj} \gg T_s$), and $T_{inj} \approx NT_s$. Then, the continuous duty cycle $d(t)$ can be discretized into $d(nT_s)$, where $n = 0, 1, 2, \dots, N-1$

$$d(nT_s) = D + \varepsilon_{inj} \sin(2\pi nT_s/T_{inj}) = D + \varepsilon_{inj} \sin(2\pi n/N). \quad (\text{A-2})$$

Therefore, $v_S(t)$ after injection is updated as

$$v_S(t) = \begin{cases} V_g, & nT_s \leq t \leq (n+d(nT_s))T_s \\ 0, & (n+d(nT_s))T_s \leq t \leq (n+1)T_s \end{cases} \quad (\text{A-3})$$

where $n = 0, \dots, N-1$, and $v_S(t)$ is a periodic function with the period of T_{inj} .

From (A-3), $v_S(t)$ includes the dc components, the harmonics of the injection frequency, and the harmonics of the switching frequency. Since $f_s \approx Nf_{inj}$, the harmonics of the switching frequency can also be seen as the harmonics of the injection frequency. Therefore, $v_S(t)$ can be rewritten as

$$v_S(t) = V_{S(0)} + \sum_{m=1}^{\infty} (a_m \cos(m\omega_{inj}t) + b_m \sin(m\omega_{inj}t)) \quad (\text{A-4})$$

where $V_{S(0)}$ is the dc component, and the integer m ($m \geq 1$) represents the m th harmonic with the fundamental frequency, f_{inj} .

From the Fourier analysis, the dc component $V_{S(0)}$ is

$$\begin{aligned} V_{S(0)} &= \int_0^{T_{inj}} v_S(t) dt / T_{inj} = \sum_{n=0}^{N-1} \left[\int_{nT_s}^{(n+d(nT_s))T_s} V_g dt \right] / T_{inj} \\ &= \sum_{n=0}^{N-1} [V_g d(nT_s)T_s] / T_{inj} = DV_g. \end{aligned} \quad (\text{A-5})$$

From the Fourier analysis, the coefficients of the m th harmonic, i.e., a_m and b_m , can be calculated below

$$a_m = (2/T_{inj}) \int_0^{T_{inj}} v_S(t) \cos(m\omega_{inj}t) dt \quad (\text{A-6})$$

$$b_m = (2/T_{inj}) \int_0^{T_{inj}} v_S(t) \sin(m\omega_{inj}t) dt. \quad (\text{A-7})$$

For calculation of a_m , substitute (A-3) into (A-6)

$$\begin{aligned} a_m &= 2/(NT_s) \sum_{n=0}^{N-1} \left[\int_{nT_s}^{(n+d(nT_s))T_s} V_g \cos(mt \cdot 2\pi/(NT_s)) dt \right] \\ &= V_g/(\pi m) \cdot \sum_{n=0}^{N-1} \left[\sin(mt \cdot 2\pi/(NT_s)) \Big|_{nT_s}^{(n+d(nT_s))T_s} \right] \\ &= V_g/(\pi m) \\ &\quad \cdot \sum_{n=0}^{N-1} [\sin(2\pi m(n+d(nT_s))/N) - \sin(2\pi mn/N)]. \end{aligned} \quad (\text{A-8})$$

From symmetry, $\sum_{n=0}^{N-1} [\sin(2\pi mn/N)] = 0$. Substitute (A-2) into (A-4)

$$\begin{aligned} a_m &= V_g/(\pi m) \\ &\quad \cdot \sum_{n=0}^{N-1} [\sin(2\pi m/N \cdot ((n+D) + \varepsilon_{inj} \sin(2\pi n/N)))] \end{aligned} \quad (\text{A-9})$$

From (A-9), a_m is a function of ε_{inj} , i.e., $f(\varepsilon_{inj})$. Since $\varepsilon_{inj} \ll D < 1$, $f(\varepsilon_{inj}) \approx f(0) + f'(0)\varepsilon_{inj}$ according to the Taylor expansion. Therefore

$$\begin{aligned} a_m &= V_g/(\pi m) \cdot \sum_{n=0}^{N-1} [\sin(2\pi m/N \cdot (n+D))] + V_g/(\pi m) \\ &\quad \cdot \sum_{n=0}^{N-1} [\cos(2\pi m/N \cdot (n+D)) \\ &\quad \cdot 2\pi m/N \cdot \sin(2\pi n/N)] \varepsilon_{inj}. \end{aligned} \quad (\text{A-10})$$

Similarly, from symmetry, $\sum_{n=0}^{N-1} \sin((2\pi m/N)(n+D)) = 0$. Therefore

$$\begin{aligned} a_m &= \varepsilon_{inj} 2V_g/N \cdot \sum_{n=0}^{N-1} [\cos(2\pi m/N \cdot (n+D)) \sin(2\pi n/N)] \\ &= \varepsilon_{inj} V_g/N \cdot \left\{ \sum_{n=0}^{N-1} [\sin(2\pi mD/N + 2\pi(m+1)n/N)] \right. \\ &\quad \left. - \sum_{n=0}^{N-1} [\sin(2\pi mD/N + 2\pi(m-1)n/N)] \right\}. \end{aligned} \quad (\text{A-11})$$

From symmetry, $\sum_{n=0}^{N-1} [\sin(2\pi mD/N + 2\pi(m \pm 1)n/N)] = 0$ for all $m \geq 1$. Therefore, the coefficient a_m is always 0.

For calculation of b_m , substitute (A-3) into (A-7)

$$\begin{aligned} b_m &= 2/(NT_s) \sum_{n=0}^{N-1} \left[\int_{nT_s}^{(n+d(nT_s))T_s} V_g \sin(mt \cdot 2\pi/(NT_s)) dt \right] \\ &= V_g/(\pi m) \cdot \sum_{n=0}^{N-1} \left[-\cos(mt \cdot 2\pi/(NT_s)) \Big|_{nT_s}^{(n+d(nT_s))T_s} \right] \\ &= V_g/(\pi m) \cdot \sum_{n=0}^{N-1} [-\cos(2\pi m(n+d(nT_s))/N) \\ &\quad + \cos(2\pi mn/N)]. \end{aligned} \quad (\text{A-12})$$

From symmetry

$$\sum_{n=0}^{N-1} \cos \frac{2\pi mn}{N} = \begin{cases} 0, & \text{if } m/N \text{ is not an integer} \\ N, & \text{if } m/N \text{ is an integer.} \end{cases} \quad (\text{A-13})$$

Therefore, due to features of the term $\cos(2\pi mn/N)$, m/N should be discussed for calculation of b_m , including m/N is not an integer and m/N is an integer.

If m/N is not an integer, substitute (A-2) and (A-13) into (A-12)

$$b_m = V_g / (\pi m) \cdot \sum_{n=0}^{N-1} [-\cos(2\pi m/N \cdot (n+D) + \varepsilon_{inj} \sin(2\pi n/N))]. \quad (\text{A-14})$$

From (A-14), b_m is also a function of ε_{inj} . Since $\varepsilon_{inj} \ll D < 1$, similarly, according to the Taylor expansion

$$b_m = V_g / (\pi m) \cdot \sum_{n=0}^{N-1} [-\cos(2\pi m/N \cdot (n+D))] + V_g / (\pi m) \cdot \sum_{n=0}^{N-1} [\sin(2\pi m/N \cdot (n+D)) \cdot 2\pi m/N \cdot \sin(2\pi n/N)] \varepsilon_{inj}. \quad (\text{A-15})$$

Similarly, from symmetry, $\sum_{n=0}^{N-1} \cos((2\pi m/N)(n+D)) = 0$. Therefore

$$b_m = \varepsilon_{inj} 2V_g / N \cdot \sum_{n=0}^{N-1} [\sin(2\pi m/N \cdot (n+D)) \sin(2\pi n/N)] = \varepsilon_{inj} V_g / N \cdot \left\{ -\sum_{n=0}^{N-1} [\cos(2\pi mD/N + 2\pi(m+1)n/N)] + \sum_{n=0}^{N-1} [\cos(2\pi mD/N + 2\pi(m-1)n/N)] \right\}. \quad (\text{A-16})$$

From symmetry, evaluate the two terms in (A-16)

$$\begin{aligned} \sum_{n=0}^{N-1} [\cos(2\pi mD/N + 2\pi(m+1)n/N)] &= 0 \\ \sum_{n=0}^{N-1} [\cos(2\pi mD/N + 2\pi(m-1)n/N)] &= \begin{cases} N \cos(2\pi D/N), & \text{if } m = 1 \\ 0, & \text{if } m \geq 2. \end{cases} \end{aligned} \quad (\text{A-17})$$

Since $N \gg 1 > D$, $2\pi D/N \approx 0$, and $\cos(2\pi D/N) \approx 1$. Therefore,

$$b_m = \begin{cases} V_g \varepsilon_{inj}, & \text{if } m = 1 \\ 0, & \text{if } m \neq 1 \text{ \& } m/N \text{ is not an integer.} \end{cases}$$

If m/N is an integer k , substitute (A-2) and (A-13) into (A-12)

$$b_m = V_g / (k\pi) - V_g / (m\pi) \cdot \sum_{n=0}^{N-1} [\cos(2\pi k \cdot ((n+D) + \varepsilon_{inj} \sin(2\pi n/N)))]]. \quad (\text{A-18})$$

From (A-18), b_m is also a function of ε_{inj} . Since $\varepsilon_{inj} \ll D < 1$, similarly, according to the Taylor expansion

$$\begin{aligned} b_m &= V_g / (k\pi) + V_g / (\pi m) \cdot \sum_{n=0}^{N-1} [-\cos(2\pi k \cdot (n+D))] \\ &\quad + V_g / (\pi m) \sum_{n=0}^{N-1} [\sin(2\pi k \cdot (n+D)) \cdot 2\pi k \cdot \sin(2\pi n/N)] \varepsilon_{inj} \\ &= V_g / (k\pi) + V_g / (\pi m) \cdot [-N \cos(2\pi kD)] \\ &\quad + V_g / (\pi m) \cdot (\sin(2\pi kD) \cdot 2\pi k) \sum_{n=0}^{N-1} [\sin(2\pi n/N)] \varepsilon_{inj}. \end{aligned} \quad (\text{A-19})$$

From symmetry, $\sum_{n=0}^{N-1} [\sin(2\pi n/N)] = 0$. Therefore, $b_m = V_g / (k\pi) [1 - \cos(2\pi kD)]$.

To sum up, the coefficients a_m and b_m are

$$\begin{cases} a_m = 0, & \text{if } m \geq 1 \\ b_m = \begin{cases} V_g \varepsilon_{inj}, & \text{if } m = 1 \\ 0, & \text{if } m \neq 1 \text{ and } m/N \text{ is not an integer} \\ V_g / (k\pi) [1 - \cos(2\pi kD)], & \text{if } k = m/N \text{ is an integer.} \end{cases} \end{cases} \quad (\text{A-20})$$

From (A-4), (A-5), and (A-20)

$$v_S(t) = DV_g + \sum_{k=1}^{\infty} V_g / (k\pi) \cdot (1 - \cos(2\pi kD)) \sin(k\omega_s t) + v_{S,inj}(t). \quad (\text{A-21})$$

REFERENCES

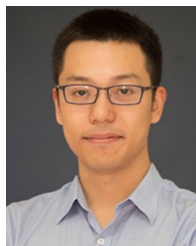
- [1] M. Chen and H. V. Poor, "High-frequency power electronics at the grid edge: A bottom-up approach toward the smart grid," *IEEE Electrific. Mag.*, vol. 8, no. 3, pp. 6–17, Sep. 2020.
- [2] Z. Gao, C. Cecati, and S. X. Ding, "A survey of fault diagnosis and fault-tolerant techniques—Part I: Fault diagnosis with model-based and signal-based approaches," *IEEE Trans. Ind. Electron.*, vol. 62, no. 6, pp. 3757–3767, Jun. 2015.
- [3] D. Li, Y. Zhao, and Y. Zhao, "A dynamic-model-based fault diagnosis method for a wind turbine planetary gearbox using a deep learning network," *Protection Control Modern Power Syst.*, vol. 7, no. 2, pp. 1–14, 2022.
- [4] A. D. Bebars, A. A. Eladl, G. M. Abdulsalam, and E. A. Badran, "Internal electrical fault detection techniques in DFIG-based wind turbines: A review," *Protection Control Modern Power Syst.*, vol. 7, no. 2, pp. 1–22, 2022.
- [5] E. Farjah, H. Givi, and T. Ghanbari, "Application of an efficient Rogowski coil sensor for switch fault diagnosis and capacitor ESR monitoring in nonisolated single-switch DC–DC converters," *IEEE Trans. Power Electron.*, vol. 32, no. 2, pp. 1442–1456, Feb. 2017.
- [6] H. Soliman, H. Wang, and F. Blaabjerg, "A review of the condition monitoring of capacitors in power electronic converters," *IEEE Trans. Ind. Appl.*, vol. 52, no. 6, pp. 4976–4989, Nov. 2016.
- [7] K. Yue, Y. Liu, X. Zhang, M. Fu, J. Liang, and H. Wang, "Transmitter-side voltage-based mutual inductances and load tracking for two-transmitter LCC-S compensated wireless power transfer systems," *IEEE J. Emerg. Sel. Topics Power Electron.*, vol. 12, no. 2, pp. 2317–2332, Apr. 2024.
- [8] A. M. R. Amaral and A. J. M. Cardoso, "A simple offline technique for evaluating the condition of aluminum–electrolytic–capacitors," *IEEE Trans. Ind. Electron.*, vol. 56, no. 8, pp. 3230–3237, Aug. 2009.
- [9] K. Yao, W. Tang, X. Bi, and J. Lyu, "An online monitoring scheme of DC-link capacitor's ESR and c for a boost PFC converter," *IEEE Trans. Power Electron.*, vol. 31, no. 8, pp. 5944–5951, Aug. 2016.

- [10] B. Wang, J. Meng, and P. Zhao, "Aging condition monitoring for aluminum electrolytic capacitor in variable speed drives," *IEEE Trans. Power Electron.*, vol. 37, no. 4, pp. 4564–4574, Apr. 2022.
- [11] L. Ren, C. Gong, and Y. Zhao, "An online ESR estimation method for output capacitor of boost converter," *IEEE Trans. Power Electron.*, vol. 34, no. 10, pp. 10153–10165, Oct. 2019.
- [12] W. Lu, X. Lu, J. Han, Z. Zhao, and X. Du, "Online estimation of ESR for DC-link capacitor of boost PFC converter using wavelet transform based time–frequency analysis method," *IEEE Trans. Power Electron.*, vol. 35, no. 8, pp. 7755–7764, Aug. 2020.
- [13] Y. Peng, S. Zhao, and H. Wang, "A digital twin based estimation method for health indicators of DC–DC converters," *IEEE Trans. Power Electron.*, vol. 36, no. 2, pp. 2105–2118, Feb. 2021.
- [14] Z. Zhao, W. Lu, P. Davari, X. Du, H. H. Iu, and F. Blaabjerg, "An online parameters monitoring method for output capacitor of buck converter based on large-signal load transient trajectory analysis," *IEEE J. Emerg. Sel. Topics Power Electron.*, vol. 9, no. 4, pp. 4004–4015, Aug. 2021.
- [15] J. Poon, P. Jain, C. Spanos, S. K. Panda, and S. R. Sanders, "Fault prognosis for power electronics systems using adaptive parameter identification," *IEEE Trans. Ind. Appl.*, vol. 53, no. 3, pp. 2862–2870, May 2017.
- [16] T. Meng and P. Zhang, "An online DC-link capacitance estimation method for motor drive systems based on an intermittent reverse-charging control strategy," *IEEE Trans. Power Electron.*, vol. 38, no. 2, pp. 2481–2492, Feb. 2023.
- [17] Z. Zhao, P. Davari, W. Lu, and F. Blaabjerg, "Online DC-link capacitance monitoring for digital-controlled boost PFC converters without additional sampling devices," *IEEE Trans. Ind. Electron.*, vol. 70, no. 1, pp. 907–920, Jan. 2023.
- [18] M. Ahmeid, M. Armstrong, S. Gadoue, M. Al-Greer, and P. Missailidis, "Real-time parameter estimation of DC–DC converters using a self-tuned Kalman filter," *IEEE Trans. Power Electron.*, vol. 32, no. 7, pp. 5666–5674, Jul. 2017.
- [19] B. X. Li and K. S. Low, "Low sampling rate online parameters monitoring of DC–DC converters for predictive-maintenance using biogeography-based optimization," *IEEE Trans. Power Electron.*, vol. 31, no. 4, pp. 2870–2879, Apr. 2016.
- [20] M. Algreer, M. Armstrong, and D. Giaouris, "Active online system identification of switch mode DC–DC power converter based on efficient recursive DCD-IIR adaptive filter," *IEEE Trans. Power Electron.*, vol. 27, no. 11, pp. 4425–4435, Nov. 2012.
- [21] M. W. Ahmad, N. Agarwal, P. N. Kumar, and S. Anand, "Low-frequency impedance monitoring and corresponding failure criteria for aluminum electrolytic capacitors," *IEEE Trans. Ind. Electron.*, vol. 64, no. 7, pp. 5657–5666, Jul. 2017.
- [22] T. Li, J. Chen, P. Cong, X. Dai, R. Qiu, and Z. Liu, "Online condition monitoring of DC-link capacitor for AC/DC/AC PWM converter," *IEEE Trans. Power Electron.*, vol. 37, no. 1, pp. 865–878, Jan. 2022.
- [23] R. Erickson and D. Maksimovic, *Fundamentals of Power Electronics*. New York, NY, USA: Springer, 2007.



Kang Yue (Student Member, IEEE) received the B.S. degree in electrical engineering and its automation from Hefei University of Technology, Hefei, China, in 2017, and the Ph.D. degree in electrical and electronic engineering from the University of the Chinese Academy of Sciences (joint program with ShanghaiTech University), Beijing, China, in 2023.

She is currently an Engineer with China Electric Power Research Institute, SGCC, Beijing. Her research interests include health monitoring and parameter identification of power electronic systems.



Haoyu Wang (Senior Member, IEEE) received the bachelor's degree (Hons.) in electrical engineering from Zhejiang University, Hangzhou, China, in 2009, and the Ph.D. degree in electrical engineering from the University of Maryland at College Park, College Park, MD, USA, in 2014.

In September 2014, he joined the School of Information Science and Technology, ShanghaiTech University, Shanghai, China, where he is currently a tenured Associate Professor. His research interests include power electronics, plug-in electric and hybrid electric vehicles, the applications of wide bandgap semiconductors, renewable energy harvesting, and power management integrated circuits.

Dr. Wang is an Associate Editor of *IEEE TRANSACTIONS ON INDUSTRIAL ELECTRONICS*, *IEEE TRANSACTIONS ON TRANSPORTATION ELECTRIFICATION*, and *CPSS Transactions on Power Electronics and Applications*.



Junrui Liang (Senior Member, IEEE) received the B.E. and M.E. degrees in instrumentation engineering from Shanghai Jiao Tong University, Shanghai, China, in 2004 and 2007, respectively, and the Ph.D. degree in mechanical and automation engineering from The Chinese University of Hong Kong, Hong Kong, China, in 2010.

He is currently an Associate Professor with the School of Information Science and Technology, ShanghaiTech University, Shanghai. His research interests include energy conversion and power conditioning circuits, kinetic energy harvesting and vibration suppression, the IoT devices, and mechatronics.

Dr. Liang is an Associate Editor of *IET Circuits, Devices and Systems* and the General Chair of the 2nd International Conference on Vibration and Energy Harvesting Applications (VEH) 2019.



Xinguo Zhang (Student Member, IEEE) received the B.S. degree in electrical engineering and automation from Fuzhou University, Fuzhou, Fujian, China, in 2019. He is currently pursuing the Ph.D. degree in power electronics with the School of Information Science and Technology, ShanghaiTech University, Shanghai, China.

His current research interests include fault diagnosis and condition monitoring of power electronic circuits.



Yu Liu (Senior Member, IEEE) received the B.S. and M.S. degrees in electrical power engineering from Shanghai Jiao Tong University, Shanghai, China, in 2011 and 2013, respectively, and the Ph.D. degree in electrical and computer engineering from Georgia Institute of Technology, Atlanta, GA, USA, in 2017.

He is currently a tenured Associate Professor with the School of Information Science and Technology, ShanghaiTech University, Shanghai. He has authored or coauthored three book chapters and more than

120 technical articles. His research interests include modeling, protection, fault location, state/parameter estimation of power systems, and power electronic systems.

Dr. Liu is a recipient of the 2023 IEEE PES Outstanding Working Group for Outstanding Technical Report Award. He is a recipient of Shanghai Eastern Scholar Professorship and Shanghai Pujiang Scholar. He serves as an Associate Editor for *IET Renewable Power Generation* (RPG) and the Guest Editor for the *Journal of Modern Power Systems and Clean Energy* (MPCE).